Tunneling and relaxation of photogenerated carriers in semiconductor quantum wells

Fumio Sasaki and Yasuaki Masumoto
Institute of Physics, University of Tsukuba, Tsukuba, Ibaraki 305, Japan
(Received 2 August 1988; revised manuscript received 17 April 1989)

The competition between tunneling (vertical transport) and relaxation (exciton formation) of photogenerated carriers in GaAs-$Al_{0.29}Ga_{0.71}As$ multiple quantum wells in an electric field has been studied by means of nonlinear luminescence and photocurrent measurements and time-correlated single-photon counting. The nonlinearity is brought about by an exciton formed by bimolecular processes. The nonlinear luminescence and photocurrent signals are qualitatively explained in terms of the competition between tunneling and relaxation. Furthermore, the heavy-exciton luminescence shows two exponential decays when the electric field is 10–29 kV/cm. The slow component is ascribed to excitons formed by the bimolecular processes as a result of multiple successive processes of tunneling, relaxation, and exciton dissociation. Under the resonant electric field $F_r = 29$ kV/cm, where electron sequential resonant tunneling occurs, the slow component diminishes because of the increase of the electron tunneling rate.

I. INTRODUCTION

The study of semiconductor quantum-well structures under an electric field lies in one of the most attractive interdisciplinary fields of fundamental physics and application. Many interesting phenomena have been discovered concerning resonant tunneling.[1–10] In particular, relaxation and tunneling of photogenerated carriers in the semiconductor quantum wells are interesting and attractive in terms of the optical spectroscopy, because we can give artificially a variety of circumstances to photogenerated carriers by designing the semiconductor microstructures.

In this work, we present the results of the study to reveal the competition between tunneling (vertical transport) and relaxation (exciton formation) of the photogenerated carriers. In the presence of an electric field along the quantum-well growth direction, some photogenerated electron-hole pairs are dissolved and fall into different wells. Some of them form excitons, while others move further to surrounding wells. The competition and the dynamical aspects of the above-mentioned processes are open problems and should be clarified. In this paper, we tried to solve the problems by means of the nonlinear luminescence[11,12] and photocurrent measurement and time-correlated single-photon counting.

II. EXPERIMENTAL PROCEDURES

In the experiments, photoexcited GaAs-$Al_{0.29}Ga_{0.71}As$ semiconductor quantum wells were studied in an electric field along the quantum-well growth direction (denoted by z direction) at 4.2 K. Samples are GaAs-$Al_{0.29}Ga_{0.71}As$ quantum wells (100 alternate periods of 12-nm GaAs wells and 5.8-nm $Al_{0.29}Ga_{0.71}As$ barriers) embedded in the p-i-n-diode structure grown by molecular-beam epitaxy.

The experimental setup for the luminescence and photocurrent measurements is shown in Fig. 1. For the photoexcitation source, a 7-ps cavity-pumped (CD) dye laser synchronously pumped by a mode-locked Kr^+ laser was used. The excitation photon energy was 1.76 eV which excites the GaAs wells selectively. The highest excitation density 480 mW cm^{-2} adopted in this study corresponds to the carrier density of 1×10^{10} cm^{-2}. A dual-chopping technique was used to study the heavy-exciton photoluminescence I_{PL} and the photocurrent I_{PC} as a function of the external electric voltage V_{ext}. The technique is suitable to detect the small nonlinearity in the photoluminescence and the photocurrent. Two equally split laser beams were chopped at different frequencies, ω_1 and ω_2. By using an optical delay, both laser beams were adjusted to hit the sample simultaneously. By using the lock-in technique, luminescence and photocurrent modulated at the frequencies ω_1, ω_2, $\omega_1+\omega_2$, and $\omega_1-\omega_2$ were separately analyzed. In the luminescence experiment, the spectrally resolved intensity of the exciton luminescence was observed by using a 75 cm monochromator and a Hamamatsu R1477 photomultiplier tube, while the spec-

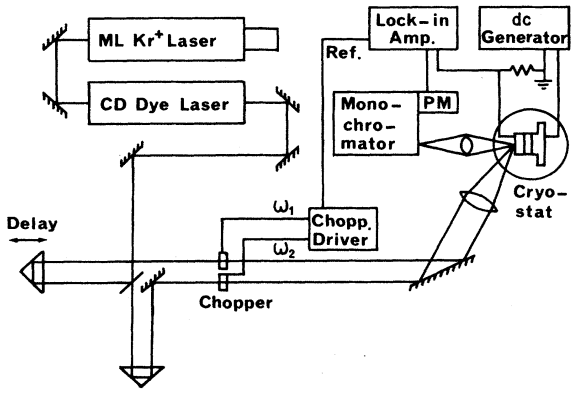

FIG. 1. Experimental setup for the nonlinear luminescence and photocurrent measurements. (PM=photomultiplier.)

trally integrated intensity was detected by replacing the monochromator by color filters. We also changed the overlap of two beams and the excitation density, as described below.

(1) The excitation pulse-repetition frequency is 4 MHz, and spot centers of two laser beams are spacially away from each other by about 300 μm.

(2) The excitation pulse-repetition frequency is 4 MHz, and two laser beam spots are completely overlapped.

(3) The excitation pulse-repetition frequency is 41 MHz, and two laser beam spots are completely overlapped.

In all cases, the spot size was about 150 μm in diameter. The spot size and the beam-overlap configuration were carefully checked by using the stereomicroscope. In the time-correlated single-photon counting experiment, the exciton luminscence peak was temporally analyzed with the time resolution of 0.4 ns and the spectral width of 0.2 nm.

III. EXPERIMENTAL RESULTS AND DISCUSSIONS

A. Excitons formed by bimolecular processes

So far, many nonlinear responses of exciton luminescence in semiconductors have been reported. Under high-density excitation, Coulomb screening, phase-space filling or exchange interaction, and band renormalization is considered to be the origin of the nonlinearity.[13] Their nonlinearity means minus deviation from the linear dependence on the excitation density. However, we observed the exciton nonlinearity under relatively low-density excitation (10^7–10^{10} cm^{-2}). In addition, the observed nonlinearity in the exciton luminescence is the plus deviation from the linear dependence on the excitation density, as described in Sec. III B. The nonlinearity is considered to come from the bimolecular exciton formation processes or the saturation of the nonradiative traps. The latter can be omitted, because the quantum yield observed in our sample is almost unity. Therefore, we consider excitons formed by bimolecular processes to interpret the nonlinearity observed in luminescence and photocurrent.

Under sufficiently low-density excitation, an exciton is formed from an electron-hole pair by monomolecular processes. The population of such monomolecular excitons is modulated at frequencies ω_1 and ω_2 in our experimental condition. On the other hand, an exciton can be formed from a pair of an electron and a hole by bimolecular processes under the elevated excitation density. The probability of bimolecular processes is proportional to the square of the excitation density.[11] Therefore, supralinearity of exciton luminescence is considered to come from the bimolecular exciton formation processes. We call this exciton the bimolecular exciton (BE). If pair dissociation or exciton mutual collision is present, the population of BE's is expected to increase. BE formation contributes to $\omega_1+\omega_2$ and $\omega_1-\omega_2$ components as well as ω_1 and ω_2 components of luminescence and photocurrent.[14] However, we can detect the BE signal selectively by measuring the $\omega_1+\omega_2$ or $\omega_1-\omega_2$ component, because the $\omega_1+\omega_2$ and $\omega_1-\omega_2$ components sensitively reflect the nonlinearity.

The detection of the nonlinear luminescence and photocurrent gives us the knowledge about the competition between tunneling and relaxation, as described below. The competition is schematically illustrated in Fig. 2. When an electron-hole pair is dissolved from an exciton by the electric field, it undergoes two processes, exciton formation and tunneling. Then, the BE luminescence intensity $I_{\mathrm{PL}}^{\mathrm{BE}}$ is expressed by the branching ratios of two processes, and described by

$$I_{\mathrm{PL}}^{\mathrm{BE}}=\frac{1/\tau_f}{1/\tau_t+1/\tau_f}n_e\ , \tag{1}$$

where $1/\tau_f$, $1/\tau_t$ and n_e denote the BE formation rate, the electron tunneling rate, and the photoexcited density, respectively. BE formation rate $1/\tau_f$ is proportional to the hole density, so that $1/\tau_f$ is proportional to the excitation density I_{ex}. On the other hand, $1/\tau_t$ depends on the electric field, but not on the excitation density. Therefore, one obtains

$$I_{\mathrm{PL}}^{\mathrm{BE}}\propto\begin{cases} I_{\mathrm{ex}} & \text{for } 1/\tau_t \ll 1/\tau_f\ , \quad (2a)\\ I_{\mathrm{ex}}^2 & \text{for } 1/\tau_t \gg 1/\tau_f\ . \quad (2b)\end{cases}$$

An intuitive explanation of the power dependence is as follows. Supposing the inequality $1/\tau_t \ll 1/\tau_f$ holds, almost all photogenerated carriers form excitons. Therefore, $I_{\mathrm{PL}}^{\mathrm{BE}}$ is proportional to the excitation density. On the other hand, if the inequality $1/\tau_t \gg 1/\tau_f$ holds, the photogenerated carriers are likely to go through the tunneling process. Therefore, $I_{\mathrm{PL}}^{\mathrm{BE}}$ is proportional to the square of the excitation density. In the following, we briefly estimate $1/\tau_t$ and $1/\tau_f$.

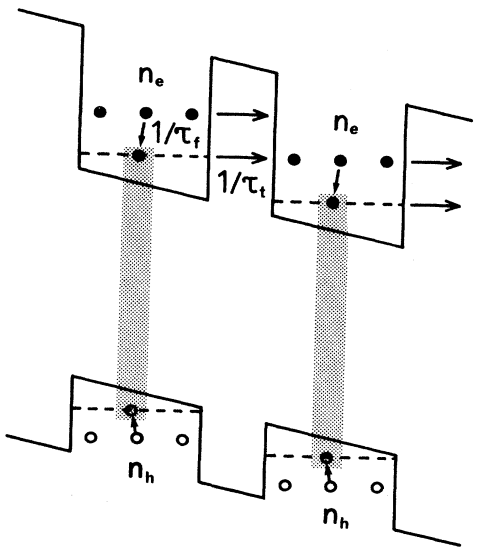

FIG. 2. Schematic illustration of the competition between tunneling and exciton formation.

The electron-tunneling rate $1/\tau_t$ was estimated by using a double-barrier transmission coefficient T_b in the Wentzel-Kramers-Brillouin (WKB) approximation.[15,16] Here, we neglected the hole tunneling, because the hole effective mass is much heavier than the electron effective mass. We used the formula $1/\tau_t = v_z T_b / 2L_z$, where $2L_z/v_z$ corresponds to the classical period of the electron motion in the quantum well, v_z is the z component of the electron velocity, and L_z the well width. The result is shown in the bottom parts of Figs. 4 and 5. In the calculation, we used the 57:43 band-gap split, corresponding to the conduction-band discontinuity of 206 meV. We also assumed the input electron kinetic energy as 55 meV in order to fit the calculated value of resonant electric field to the experimental one of 29 kV/cm.

To estimate the BE formation rate $1/\tau_f$, we used a two-dimensional collision model for a rigid disk. An electron tunneling to the next well moves along the layer, collides with a hole, and forms an exciton. In this model the BE formation rate is expressed by

$$1/\tau_f = 2n_e a_B v_0, \quad v_0 = v_e - v_h \ , \tag{3}$$

where a_B and v_e (v_h) denote the exciton Bohr radius ($=13.6$ nm) and electron (hole) velocity, respectively. Here, the hole density is assumed to be equal to the electron density. If the electron-hole system is in thermal equilibrium with the lattice, v_i ($i=e,h$) corresponds to the thermal velocity. In the presence of an electric field, however, the carrier system is considered to be hot and v_i is assumed to be represented by $(2eFd/m_i)^{1/2}$, where d and m_i ($i=e,h$) denote one period of the superlattice and the effective mass ($m_e = 0.067 m_0$ for an electron and $m_h = 0.34 m_0$ for a heavy hole), respectively.[9] This assumption is wrong if the BE formation rate is smaller than the hot-carrier cooling rate. However, the upper limit of the BE formation rate is estimated in this way. In the excitation condition (1), two beams are spacially away from each other, so that BE formation rate $1/\tau_f$ is considered to be slower than that in excitation condition (2). In this case, BE formation rate observed in the $\omega_1+\omega_2$ component is estimated by using the carrier density at the center position of two beams in the excitation condition (1). We assumed the spatial carrier distribution to have a Gaussian profile, because the laser beam has a Gaussian profile.

B. Nonlinear luminescence and photocurrent

Photoluminescence spectra of the sample under the external electric voltage are shown in Fig. 3, which is similar to that already reported in Ref. 5. Figures 4 and 5 show the heavy-exciton luminescence intensity and photocurrent as a function of external electric voltage under the excitation conditions (1) and (2), respectively. Here, the electric field F estimated by the Stark shift of the heavy-exciton luminescence peak is shown as the uppermost scale.[2,5] The top parts in Figs. 4 and 5 show ω_1 components of I_{PL} and I_{PC} versus V_{ext}. Two steplike changes are observed in the curves of I_{PL} and I_{PC}. The

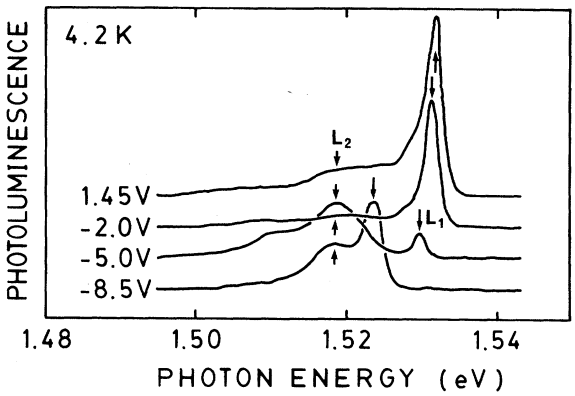

FIG. 3. Photoluminescence spectra of the sample under the external electric voltage. The electric field F is estimated to be 4, 18, 28, and 53 kV/cm for the applied voltages $+1.45$, -2.0, -5.0, and -8.5 V from the Stark shift of the heavy-exciton luminescence. The peak L_1 indicated by a long arrow is the heavy-exciton luminescence from the multiple-quantum-well structures and the peak L_1 indicated by a short arrow is the luminescence from the GaAs cap layer.

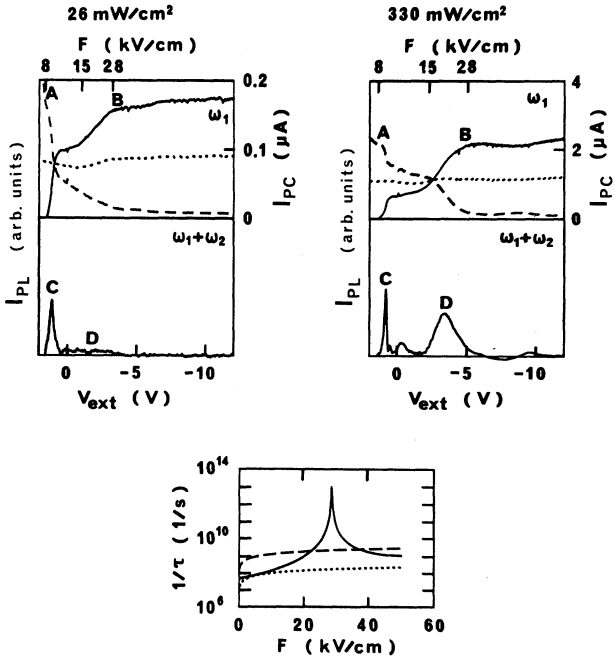

FIG. 4. Heavy-exciton luminescence intensity and photocurrent observed in GaAs-$Al_{0.29}Ga_{0.71}As$ multiple quantum wells as a function of external electric voltage in the excitation condition (1) (4 MHz, bad overlap) described in the text. The upper parts represent ω_1 component of I_{PL} (dashed line), I_{PC} (solid line), and $(I_{PL}+I_{PC})/2$ (dotted line). The middle parts represent $\omega_1+\omega_2$ component of I_{PL}. The bottom part is the calculated result of BE formation rate $1/\tau_f$ and the tunneling rate $1/\tau_t$. Dotted and dashed lines show $1/\tau_f$ at 26 mW/cm^2 and 330 mW/cm^2 excitation, respectively. The solid line shows $1/\tau_t$.

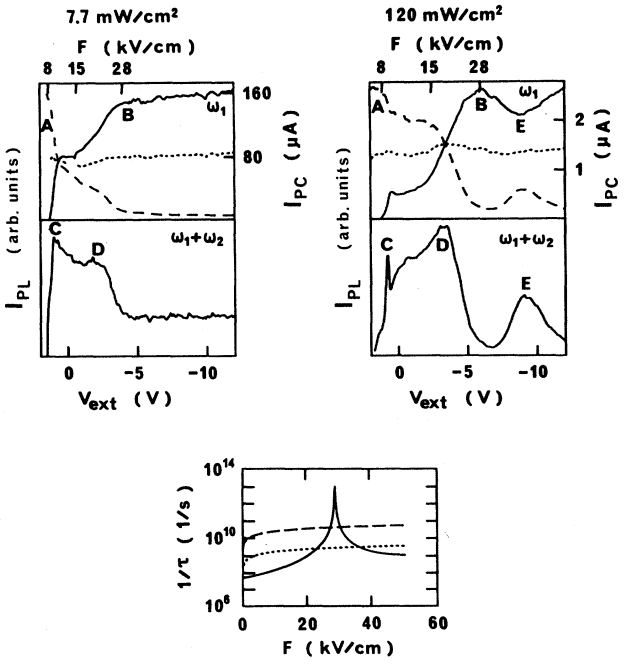

FIG. 5. Heavy-exciton luminescence intensity and photocurrent observed in GaAs-$Al_{0.29}Ga_{0.71}As$ multiple quantum wells as a function of external electric voltage in the excitation condition (2) (4 MHz, good overlap) described in the text. The upper parts represent ω_1 component of I_{PL} (dashed line), I_{PC} (solid line), and $(I_{PL}+I_{PC})/2$ (dotted line). The middle parts represent $\omega_1+\omega_2$ component of I_{PL}. The bottom part is the calculated result of BE formation rate $1/\tau_f$ and the tunneling rate $1/\tau_t$. Dotted and dashed lines show $1/\tau_f$ at 7.7 mW/cm^2 and 120 mW/cm^2 excitation, respectively. The solid line shows $1/\tau_t$.

steplike changes B ($F=28$ kV/cm) and A ($F=8$ kV/cm) are identified to be electron sequential resonant tunneling and exciton dissociation followed by electron tunneling, respectively.[3,6] Between two steplike changes there is a plateau. With the increase of the excitation density, I_{PL} increases supralinearly, while I_{PC} increases sublinearly at the plateau region. Here, we note that the nonlinearity for the excitation density is observed in the same electric field F. Therefore, the nonlinearity cannot be explained in terms of the field screening.[10] If a constant multiplies I_{PL} so as to equalize the maximum of I_{PL} to the maximum of I_{PC}, the sum of both signals is almost independent of V_{ext}, as shown in Figs. 4 and 5. This means that photocurrent behaves as a complement of luminescence.[7] Taking account of the absorption and reflection of incident light at the cap layer, the carrier number excited in all the quantum wells is estimated to be 2×10^{13} s^{-1} in the case of the right-hand side of Fig. 5. The value corresponds to 3 μA. This agrees with the measured maximum of I_{PC} within an order of magnitude. This means that almost all the photogenerated carriers contribute to luminescence or photocurrent.

The middle parts of Figs. 4 and 5 show the $\omega_1+\omega_2$ component of I_{PL}. Prominent structures C and D are seen in the $\omega_1+\omega_2$ component in both Figs. 4 and 5. A structure E is seen in Fig. 5, while not in Fig. 4. In the excitation condition (3), the $\omega_1+\omega_2$ component of I_{PL} shows almost the same profile as those in the excitation condition (2) shown in Fig. 5. The $\omega_1+\omega_2$ component of I_{PC} has almost the same profile with I_{PL}, because the increase of photoluminescence corresponds to decrease of photocurrent in the $\omega_1+\omega_2$ component.[7] By moving the optical delay, we can obtain the temporal information about the $\omega_1+\omega_2$ component. The $\omega_1+\omega_2$ components of I_{PL} and I_{PC} were found to change little within 3 ns of the pulse separation.

The excitation-density dependences of structures C, D, and E are different from one another. They depend on the excitation conditions. Figures 6, 7, and 8 show the excitation-density dependences of C, D, and E under the conditions (1), (2), and (3), respectively.[17] In the excitation condition (1), the intensity of C was found to be almost proportional to I_{ex} and that of D was found to be almost proportional to I_{ex}^2.[7] Two asymptotic expressions in Eq. (2) hold for C and D, respectively. In the excitation condition (2), on the other hand, the excitation-density dependences of each structure are more complicated and do not follow the simple power law. The excitation-density dependence of structures C, D, and E in turn grows stronger. In the excitation condition (3), the intensities of C and D are found to be almost proportional to I_{ex}. The excitation-density dependence of E is similar to that in the excitation condition (2).

Now, we can explain the excitation-density dependences of the $\omega_1+\omega_2$ signal by using the bimolecular exciton model described in Sec. III A. In the excitation condition (1), the carrier density contributing to the $\omega_1+\omega_2$ component is small enough, so that BE formation rate is slower than the tunneling rate, as shown in the bottom part of Fig. 4. Then, Eq. (2b) holds around the structure D. In the excitation condition (2), the carrier density

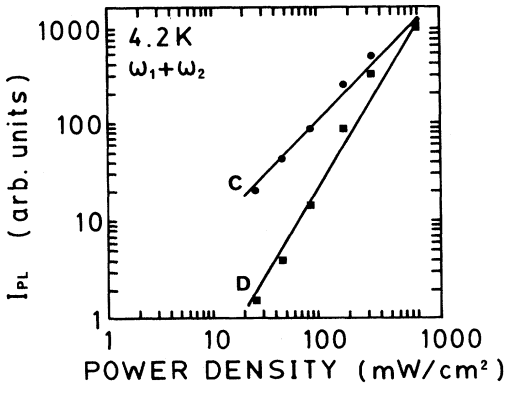

FIG. 6. Power dependences of the structure of C (solid circles) and D (solid squares) under the excitation condition (1). Power dependences of C and D are expressed by $I_{ex}^{1.1}$ and $I_{ex}^{1.8}$, respectively.

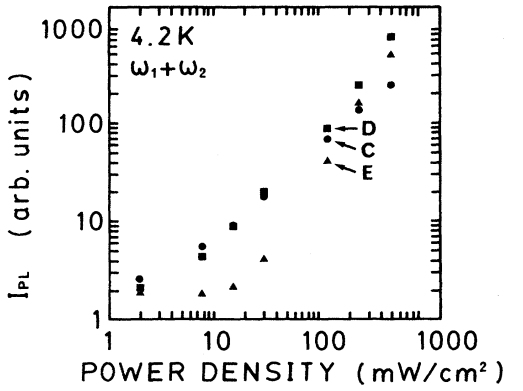

FIG. 7. Power dependences of the structure of C (solid circles), D (solid squares), and E (solid triangles) under the excitation condition (2).

contributing to the $\omega_1+\omega_2$ component is large enough, so that BE formation rate is comparable with the tunneling rate under low-density excitation and faster than the tunneling rate under high-density excitation, except for the case of the resonant tunneling. Then, Eq. (2b) no longer holds around the structure D. In the resonant tunneling case, BE is not formed as a result of the resonant enhancement of the electron tunneling rate. Therefore the dip between D and E in Fig. 5 arises.

In the excitation condition (3), the carrier density excited by one pulse is smaller than the excitation conditions (1) and (2), but temporal as well as spatial overlap of two beams was good, because the excitation pulse-repetition rate is ten times larger than that in other two conditions. Then, BE is formed from an electron (a hole) generated by a pulse and a hole (an electron) generated by the next pulse, so that BE formation rate $1/\tau_f$ is considered to be faster than electron tunneling rate $1/\tau_t$ when the electric field is below 28 kV/cm. Therefore, the

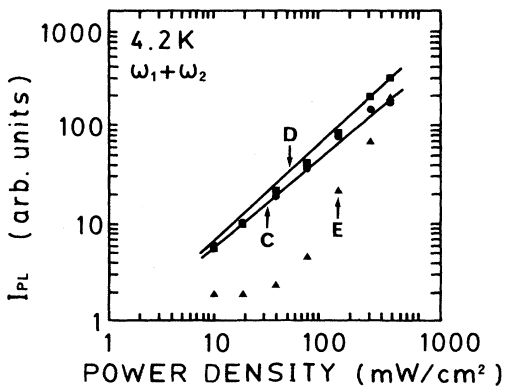

FIG. 8. Power dependences of the structure of C (solid circles), D (solid squares), and E (solid triangles) under the excitation condition (3). Power dependences of C and D are expressed by $I_{ex}^{0.92}$ and $I_{ex}^{1.1}$, respectively.

intensities of C and D are proportional to I_{ex} in the case of condition (3), following the Eq. (2a).

When the excitation density is high enough, the structure E is observed in the ω_1 and $\omega_1+\omega_2$ components (see the right part of Fig. 5). This implies that BE formation rate is comparable to or faster than the tunneling rate at $F=42$ kV/cm, as expected from the calculated results (see the bottom parts of Figs. 4 and 5). Then, some BE's are formed at $F=42$ kV/cm, and the structure B in the ω_1 component makes a peak in the high-density excitation. Under low-density excitation the BE formation rate is much slower than the tunneling rate, so that the structure E is not observed.

We noted that BE formation also contributes ω_1 and ω_2 components of I_{PL} and I_{PC}.[14] In order to see this feature more clearly, we define the critical electric field F_c at which the ω_1 components of I_{PL} and I_{PC} are equal to each other. The critical field F_c depends on the excited carrier density, as shown in Fig. 9. With the increase of the excited carrier density, F_C increases like a step. Further, the ω_1 components of I_{PL} and I_{PC} at F_c were found to be proportional to the excitation density, independent of the excitation conditions.

At the critical field F_c, the electron tunneling process equilibrates with the exciton formation process, so that the ratio of the electron tunneling rate to the exciton formation rate is considered to be constant. Therefore, it is reasonable that ω_1 components of I_{PL} and I_{PC} at F_c are proportional to the excitation density, as is expected from Eq. (1). The increase of F_c as well as supralinearity of I_{PL} for the excitation density is explained by the formation of BE. When the excitation density is low, BE formation is small. Then, it is considered that the once-formed excitons do not dissociate and go through radia-

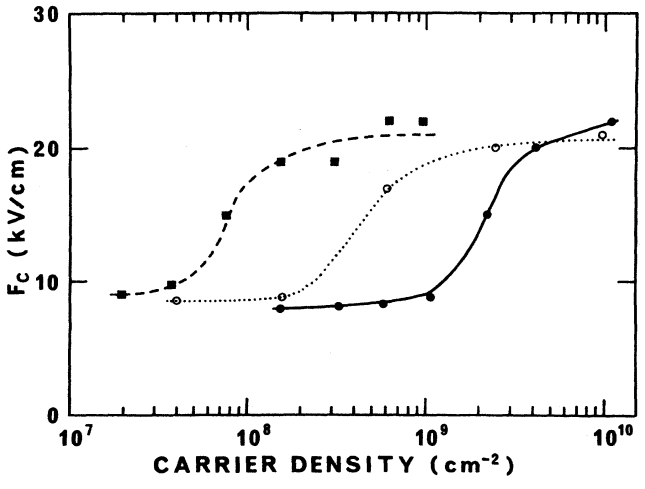

FIG. 9. Critical field F_c vs the excited carrier density. Solid circles correspond to the excitation condition (1) (4 MHz, bad overlap), open circles to the excitation condition (2) (4 MHz, good overlap), and solid squares to the excitation condition (3) (4 MHz, good overlap), respectively. Lines are guides for eyes.

tive recombination below 10 kV/cm. On the other hand, the higher the excitation density, the faster BE formation. Therefore, the high field is required in order to equalize the carriers contributing to photocurrent to those contributing to photoluminescence. The reason why the F_c does not increase beyond 20 kV/cm is ascribed to the resonant enhancement of $1/\tau_t$.

So far, we have explained the results of nonlinear luminescence and photocurrent experiment in terms of the BE model, but another possibility may exist. It is the field-screening effect by the photoexcited carriers. If the slight difference in the electric field between under irradiation of two beams and under that of one beam exists, the difference is reflected in the nonlinear component in differential form as $dI_P/dF\delta F$, where $(P=\mathrm{PL,PC})$. Here, F denotes the electric field and δF denotes the field difference. The field difference was estimated experimentally and quantitatively. As a result, it was found to be smaller than that of our detection limit which is about 1 kV/cm. Thus we omitted the possibility. Anyway, it is impossible to explain our results qualitatively and systematically in terms of the field screening.

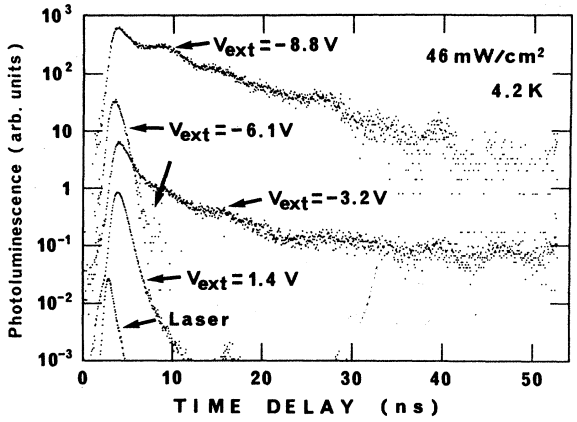

FIG. 10. Temporal profile of the heavy-exciton luminescence obtained by time-correlated single-photon counting. The estimated electric fields in the multiple quantum wells are 0, 22, 28, 42 kV/cm for the applied voltages of 1.4, −3.2, −6.1, −8.8 V, respectively.

C. Time-resolved luminescence

A time-resolved luminescence measurement also gives us useful information about the competition between tunneling and relaxation.[5,7] Figure 10 shows the results of time-resolved heavy-exciton luminescence under the excitation condition (2). When the electric field F is between 10 and 29 kV/cm, the temporal change of the heavy-excition luminescence consists of two decay components. The fast one decays in several hundred picoseconds, and the slow one in several tens of nanoseconds, depending on the electric field and excitation density. The slow component is considered to be ascribed to the luminescence of BE formed as a result of the repetitions of exciton dissociation, electron tunneling, and exciton formation. In fact, in the flat-band condition ($V_{\mathrm{ext}}=1.6\pm0.2$ V) the slow component is not seen. The results are consistent with those of time-resolved nonlinear luminescence and photocurrent experiment. Because of the slow decay due to BE, nonlinear components of I_{PL} and I_{PC} change little within 3 ns.

At the resonant field of $F_r=2.9\times10^4$ V/cm, where electron sequential resonant tunneling occurs, the slow decay component diminishes. This is because the electron tunneling rate is fast enough not to form BE's as expected from the calculation shown in bottom parts of Figs. 4 and 5. The same phenomena were also observed consistently in the same sample by the time-resolved photocurrent measurement.[8] Above F_r, the single long-decay component is observed only under the relatively high-density excitation (>40 mW cm^{-2}). In this condition BE luminescence alone is observed, because BE formation rate is faster than the tunneling rate. On the other hand, under the low-density excitation (<10 mW cm^{-2}) the exciton luminescence is not seen above F_r. This is because BE formation rate is much slower than the tunneling rate. These time-resolved results are consistent with the results obtained by the nonlinear luminescence and photocurrent spectroscopy.

IV. CONCLUSIONS

We investigated the competition between tunneling and relaxation of photogenerated carriers in GaAs-$Al_{0.29}Ga_{0.71}As$ multiple quantum wells in a perpendicular electric field by using nonlinear luminescence and photocurrent and time-correlated single-photon counting. We considered an exciton formed by the bimolecular processes to explain the results. BE gives the characteristic features observed in the nonlinear luminescence and photocurrent. It also gives the slow-decay component to the heavy-exciton time-resolved luminescence. The slow-decay component diminishes at the condition of the sequential resonant tunneling because the electron-tunneling rate is overwhelmingly faster than the exciton formation rate. The change of nonlinear luminescence and photocurrent as a function of the excitation density is explained in terms of the competition between tunneling and relaxation. The time-resolved results are also explained consistently in terms of the competition between tunneling and relaxation.

ACKNOWLEDGMENTS

The authors would like to thank Dr. H. Okamoto at Furukawa Electric Co. and Dr. S. Tarucha at Nippon Telegraph and Telephone Co. for providing high-quality samples. This work was supported by a Grant-in-Aid for Scientific Research No. 62460022 from the Ministry of Education, Science and Culture of Japan. It was also supported by the Mitsubishi Foundation.

[1]R. Tsu and L. Esaki, Appl. Phys. Lett. **22**, 562 (1973).
[2]G. Bastard, E. E. Mendez, L. L. Chang, and L. Esaki, Phys. Rev. B **28**, 3241 (1983).
[3]F. Capasso, K. Mohammed, and A. Y. Cho, IEEE J. Quantum Electron. **QE-22**, 1853 (1986).
[4]H.-J. Polland, K. Kohler, L. Schultheis, J. Kuhl, O. Göbel, and C. W. Tu, Superlatt. Microstruct. **2**, 309 (1986).
[5]Y. Masumoto, S. Tarucha, and H. Okamoto, Phys. Rev. B **33**, 5961 (1986).
[6]Y. Masumoto and F. Sasaki, J. Lumin. **40/41**, 709 (1987).
[7]Y. Masumoto and F. Sasaki, J. Lumin. **38**, 285 (1987).
[8]S. Tarucha, K. Ploog, and K. von Klitzing, Phys. Rev. B **36**, 4558 (1987).
[9]R. C. Miller, D. A. Kleinman, and A. C. Gossard, Phys. Rev. B **29**, 7085 (1984).
[10]J. A. Kash, E. E. Mendez, and H. Morkoç, Appl. Phys. Lett. **46**, 173 (1985).
[11]D. von der Linde, J. Kuhl, and E. Rosengart, J. Lumin. **24/25**, 675 (1981).
[12]D. Rosen, A. G. Doukas, Y. Budansky, A. Katz, and R. R. Alfano, Appl. Phys. Lett. **39**, 935 (1981).
[13]*Optical Nonlinearities and Instabilities in Semiconductors,* edited by H. Haug (Academic, New York, 1988).
[14]Here, we note that the BE formation gives ω_1 and ω_2 components as well as $\omega_1+\omega_2$ and $\omega_1-\omega_2$ components to photoluminescence and photocurrent. BE population is represented by the product of electron and hole densities. In our experiment, the electron and hole densities are modulated at frequencies ω_1 and ω_2. If we take account of up to the second term in Fourier components, the temporal change of both the densities are approximately expressed by $n_1(1+\cos\omega_1 t)+n_2(1+\cos\omega_2 t)$, because the modulation has the form of an on-off wave. Here, n_i $(i=1,2)$ represents the carrier density excited by ω_i light. As a result, the product of electron and hole densities gives the ω_1, ω_2, $2\omega_1$, $2\omega_2$, $\omega_1+\omega_2$, and $\omega_1-\omega_2$ components.
[15]R. H. Davis and H. H. Hosack, J. Appl. Phys. **34**, 864 (1963).
[16]D. Bohm, *Quantum Theory* (Prentice-Hall, Englewood Cliffs, New York, 1951), Chap. 12.
[17]Here, we note that $1/\tau_f$ depends on the overlap of two beams and the excitation density and that the change of the $1/\tau_f$ varies all of the ω_1, ω_2, $\omega_1+\omega_2$, and $\omega_1-\omega_2$ components. The ω_1 and ω_2 components do not seriously depend on the overlap of the two beams, while $\omega_1+\omega_2$ and $\omega_1-\omega_2$ components seriously depend on it. This is because the $\omega_1+\omega_2$ and $\omega_1-\omega_2$ components selectively reflect the BE that is formed by an electron (a hole) excited by one beam and a hole (an electron) excited by another.